HHS Public Access

Author manuscript

Vis Neurosci. Author manuscript; available in PMC 2016 July 01.

Published in final edited form as:

Vis Neurosci. 2016 January ; 33: E001. doi:10.1017/S0952523815000310.

Multi-nucleate retinal pigment epithelium cells of the human macula exhibit a characteristic and highly specific distribution

Austin C Starnes[1], **Carrie Huisingh**[1], **Gerald McGwin Jr.**[2], **Kenneth R Sloan**[3,1], **Zsolt Ablonczy**[4], **R. Theodore Smith**[5], **Christine A Curcio**[1], and **Thomas Ach**[1,6]

[1]University of Alabama at Birmingham, Department of Ophthalmology, Birmingham, AL, USA

[2]University of Alabama at Birmingham, Department of Epidemiology, Birmingham, AL, USA

[3]University of Alabama at Birmingham, Department of Computer and Information Sciences, Birmingham, AL, USA

[4]Medical University of South Carolina, Department of Ophthalmology, Charleston, SC, USA

[5]New York University School of Medicine, Department of Ophthalmology, New York, NY, USA

[6]University Hospital Würzburg, Department of Ophthalmology, Würzburg, Germany

Abstract

Background—The human retinal pigment epithelium (RPE) is reportedly 3% bi-nucleated. The importance to human vision of multi-nucleated (MN)-RPE cells could be clarified with more data about their distribution in central retina.

Methods—Nineteen human RPE-flatmounts (9≤51years, 10>80 years) were imaged at 12 locations: 3 eccentricities (fovea, perifovea, near periphery) in 4 quadrants (superior, inferior, temporal, nasal). Image stacks of lipofuscin-attributable autofluorescence and phalloidin labeled F-actin cytoskeleton were obtained using a confocal fluorescence microscope. Nuclei were devoid of autofluorescence and were marked using morphometric software. Cell areas were approximated by Voronoi regions. Mean number of nuclei per cell among eccentricity/quadrant groups and by age were compared using Poisson and binominal regression models.

Results—A total of 11403 RPE cells at 200 locations were analyzed: 94.66 % mono-, 5.31% bi-, 0.02% tri-nucleate, and 0.01% with 5 nuclei. Age had no effect on number of nuclei. There were significant regional differences: highest frequencies of MN-cells were found at the perifovea (9.9%) and near periphery (6.8%). The fovea lacked MN-cells almost entirely. The nasal quadrant had significantly more MN-cells compared to other quadrants, at all eccentricities.

Conclusion—This study demonstrates MN-RPE cells in human macula. MN-cells may arise due to endoreplication, cell fusion, or incomplete cell division. The topography of MN-RPE cells follows the topography of photoreceptors; with near-absence at the fovea (cones only) and high

Corresponding author: Thomas Ach, MD, University Hospital Würzburg, Dept of Ophthalmology, Josef-Schneider-Straße 11, 97080 Würzburg, Germany, P: +49-931-2010, F: +49-931-201-20245; ach_t@ukw.de.

Competing interests

None of the authors has any potential conflict to report.

No conflicting relationship exists for any author.

frequency at perifovea (highest rod density). This distribution might reflect specific requirements of retinal metabolism or other mechanisms addressable in further studies.

Keywords

retinal pigment epithelium; cell nucleus; bi-nucleate; multi-nucleate

Introduction

The retinal pigment epithelium (RPE) is a highly specialized and polarized cell monolayer of the retina. Major RPE functions important for the adjacent photoreceptors and choroid include phagocytosis of photoreceptor outer segments, absorption of excess light, processing of retinoids for phototransduction (visual cycle), maintenance of the blood–retina barrier, and secretion of growth factors, cytokines, and lipoprotein particles (Strauss, 2005; Shi *et al.*, 2008; Wang *et al.*, 2009). The overlying photoreceptors show a characteristic distribution in humans, which reflects different requirements for vision: cones only in the fovea, highest rod density in the perifovea, and highest rod:cone ratio in the near periphery (Curcio *et al.*, 1990).

The majority of cells in the human body have one nucleus and only a few cell types are multi-nucleated (Lacroix & Maddox, 2012). In a classic 1967 study by Ts'o and Friedman, 3% of RPE cells in humans were reported bi-nucleate (Ts'o & Friedman, 1967). Precise information about spatial distribution of bi-nucleate RPE cells in the human RPE is rare since information about exact measurement position is unavailable (Ts'o & Friedman, 1967) or imprecisely reported with regard to distance from the fovea.(Robb, 1985) Robb et al. described regional differences in bi-nucleate cell density in the developing human eye, with highest density (4.7 %, range 1.7 to 11.4 %) at the equator; however, no numbers for macula were reported. Multi-nucleate cells in some tissues may have a protective role in stressed and cancer cells (Lacroix & Maddox, 2012; Pandit *et al.*, 2013). The significance of multi-nucleate cells in the human RPE is not understood, and an accurate description of their topography would be informative.

In histological autofluorescence images of the RPE, cell nuclei appear as non-fluorescent intracellular structures (Bodenstein & Sidman, 1987). In our recent study of histological autofluorescence in RPE flat-mounts (Ach *et al.*, 2014), we noted that cell nuclei were devoid of autofluorescence and thus clearly silhouetted against the bright autofluorescence signal of lipofuscin and melanolipofuscin. Here, we used these images to systematically examine the macula and near periphery of human RPE flatmounts to determine the number of nuclei per cell, at different eccentricities and quadrants. We found a characteristic distribution of multi-nucleate cells that might reflect the adaptation of RPE cells to the special needs of overlying photoreceptors.

Materials and Methods

The Institutional Review Board at the University of Alabama at Birmingham approved the use of human tissue. All methods conformed to the guidelines of the Declaration of Helsinki.

Tissues

RPE-flatmount tissues were collected from eyes of white donors to the Alabama Eye Bank recovered within 4.2 hours of death (median 2.3 hours) (Ach *et al.*, 2014). Briefly, RPE-Bruch's membrane (BrM) flatmounts were prepared from chorioretinal tissue (~20- to 25-mm total width and including optic disc, macula, and retinal vascular arcades) by removing retina and choroid in a multistep, photodocumented process. The filamentous actin of the RPE cells was labeled with (Alexa Fluor 647 phalloidin (#A22287; Life Technologies, Grand Island, NY, USA). Tissues were mounted (#P36930, ProLong Gold anti-fade reagent; Molecular Probes, Eugene, OR, USA) with BrM down on microscope slides (#12-550-15; Fisher Scientific, Pittsburgh, PA, USA), and cover slipped (#061812-9; Fisher Scientific). (Ach *et al.*, 2014)

The absence of chorioretinal pathologies in all tissues was determined by gross inspection under a dissection microscope using trans- and oblique epi-illumination. Additional ex vivo spectral domain optical coherence tomography and AF images (Spectralis, Heidelberg Engineering, Heidelberg, Germany) corroborated these assessments, for 15 tissues.

Imaging acquisition and sampling

The imaging procedure and data acquisition were described in detail (Ach *et al.*, 2014). Briefly, fluorescence imaging was performed using a BX51 microscope (Olympus, Center Valley, PA, USA) with a motorized stage control, oil objective (UPlanApo 340 oil iris, numerical aperture 1.0; Olympus), digital camera (Orca R2, Hamamatsu, Middlesex, NJ, USA), excitation light source emitting a mercury arc lamp spectrum (Xcite 120Q, Lumen Dynamics Group Inc., Mississauga, Ontario, Canada), and filter cubes for cytoskeleton imaging (LF635-B-000, excitation 635 nm, emission >650 nm; Semrock Inc., Rochester, NY, USA) and AF lipofuscin/ melanolipofuscin imaging (Long-pass GFP filter cube OSF-GFP-30LP-B-Z, excitation: 460–490 nm, emission >505 nm, Semrock Inc.), all under control of the integrated microscope software (cellSens Dimension V1.7.1; Olympus). Tissues were imaged at 0.4 μm steps in the z-direction. For each tissue, images were taken at 75 to 90 predefined locations in an unbiased sampling pattern centered on the foveola and covering eccentricities from zero to 10 mm.

For the current study, AF and cell cytoskeleton data sets from 19 (two age groups: ≤ 51 years (9 donors) and > 80 years (10 donors)) of the previously 20 imaged tissues were used. In one tissue nuclei were hardly visible and thus was not included in the analysis. From each tissue data set, images were chosen in one of 12 locations: three eccentricities (within 0.5 mm from foveal center), perifovea (4 mm distance to foveola), and periphery (10 mm distance to foveola)) at four quadrants (superior, inferior, nasal, and temporal). Based on our previous findings, these areas sample the varying photoreceptor populations serviced by RPE (fovea: cones only; perifovea: highest rod density; near periphery: highest rod/cone ratio) (Curcio *et al.*, 1990; Ach *et al.*, 2014).

Nucleus determination and analysis

From the 228 possible locations (19 tissues x 12 locations), 28 locations were omitted from further analysis due to poor image quality or preparative tissue losses. Therefore, nuclei were counted in the remaining 200 locations.

We used the z-stacks of autofluorescence images (488 nm excitation) to view an autofluorescence-devoid region in each cell, as described (Bodenstein & Sidman, 1987). Z-stacks were overlaid with a Voronoi diagram representing each cell (Figure 1). To record nuclear position, we used a custom FIJI plugin (http://fiji.sc; plugin available from the authors upon request) (Figure 1). A trained observer (AS) scrolled through image z-stacks at each location to find the best focus for the nucleus of each cell and place a mark indicating "*definitely present*" at its center. While rolling focus through a z-stack, all cellular boundaries could be seen. Nuclei close to cell borders were assigned to the cell body that covered the largest part of the nuclei. Cells lacking visible nuclei were marked as *"cannot determine"*. This category included those that had an artifact obscuring visualization, cells that were hypo-autofluorescent due to a high density of melanosomes, and nuclei that could not be distinguished from the cytoplasm. We included for analysis only those locations with *"definitely present"* greater than 85 %. This led to elimination of 4 locations, for a total of 196 locations to be analyzed.

Statistics

For analysis, percentage of multi-nucleate cells and nuclei per cell were determined. Poisson regression models using generalized estimating equations (GEE) were used to compare the mean number of nuclei per cell by age group, eccentricity, and quadrant. The exchangeable correlation structure was imposed, which models equal correlations between each location; this structure produced better-fit statistics than other correlation structures (Ziegler *et al.*, 1998). To test this association, model-based and empirical standard errors (SEs) were calculated. Results were similar between the empirical and model-based, so for consistency p-values are presented from the empirical SE models only. The analysis was repeated using a binomial regression model with a binary outcome (0=cell had 1 nucleus, 1=cell had >1 nucleus). Lastly, Spearman correlations were used to assess the linearity between the number of nuclei, cell area, AF, and number of neighbors. P-values <0.05 were considered statistically significant.

Results

Nineteen macula RPE-BrM flatmounts (9 ≤ 51 years, 10 > 80 years) were imaged at 196 locations (Supplementary Figure 1) in an unbiased and predefined pattern, and a total of 11403 cells were interrogated (Table 1). Of these, 94.7 % (10797 cells) were mono-nucleate, and 5.31 % (606 cells) were bi-nucleate. Two cells (0.02 %) had three and one cell (0.01 %) had five nuclei, respectively (Figure 2). There was no significant difference between the two age groups, either in the percentage of multi-nucleate cells (p=0.79) or the mean number of nuclei per cell (both ~1.05 nuclei per cell, p=0.83). As reported earlier, we detected no evidence for overall reduction in RPE cell density between the two age groups, consistent with collectively inconclusive age-effects reported by other investigators (Ach *et al.*, 2014).

Significant differences in number of multi-nucleate cells were detectable between eccentricities fovea, perifovea, and periphery (Table 2, Figure 3, Supplementary Figure 1). Perifovea had the highest mean number of nuclei per cell, followed by periphery and fovea (1.10, 1.07, 1.01, respectively; Table 1). At the perifovea, a significantly higher percentage of multi-nucleate RPE cells (9.89 %) were found compared to fovea (0.74 %, p=<0.001) and periphery (6.57 %, p=<0.0001).

There was also a significant difference between the nasal quadrant and the inferior, superior, and temporal quadrants. The nasal quadrant had the highest mean number of nuclei per cell (1.08) while the inferior, superior, and temporal quadrants had similar means (~1.04). Quadrant analysis revealed highest percentage of multi-nucleate cells nasal (8.32 %), followed by inferior (4.85 %), superior (4.29 %), and temporal (4.07 %) quadrant (Table 1). Comparisons by quadrant and eccentricity are shown in Table 2.

There was a weak positive correlation between area, number of neighbors and total AF/cell with number of nuclei. It was our impression that some cell nuclei in multi-nucleate cells were smaller than nuclei in surrounding cells (Figure 2D).

Discussion

This is the first study examining the spatial distribution of multi-nucleate RPE cells of the human macula in a systematic and unbiased sampling pattern. Highest densities of multi-nucleate cells are found at the perifovea, which identifies a close relationship to the distribution and metabolism of overlying rod photoreceptors. Remarkably, the lowest densities were consistently found for the fovea, suggesting that minimal perturbations from perfect geometry confer a selective advantage for foveal cone vision (Hirsch & Curcio, 1989).

Differences between humans and laboratory animals in RPE polyploidy

Among mammals, bi-nucleate RPE cells are reported for mice, rats,, monkeys, and humans (Ts'o & Friedman, 1967). Rodents have a high percentage of bi-nucleate cells (up to 85 %) (Ts'o & Friedman, 1967), that is attained shortly after birth (Bodenstein & Sidman, 1987). Bi-nucleate RPE in rodents exhibit spatial differences: 70 % of cells in the center are bi-nucleate (Al-Hussaini *et al.*, 2008), while this number declines to 25 % in the periphery (Bodenstein & Sidman, 1987). Frequency of bi-nucleate RPE cells in humans and monkeys seems to be identical (Ts'o & Friedman, 1967), however, reports are rare and while a few snapshots of bi- or multi-nucleate cells in humans are available in the literature (Feeney, 1978; Al-Hussaini *et al.*, 2008; Al-Hussaini *et al.*, 2009; Ding *et al.*, 2011), no systematic analysis exists so far. In two histological studies hydrogen peroxide bleached, hematoxylin eosin stained RPE flatmounts were used to report multi-nucleate RPE cells. Ts'o and Friedman found only 3 % bi-nucleate RPE cells in humans (Ts'o & Friedman, 1967) viewed at unspecified regions. Later, Robb et al found that during ocular development (gestational week 25 – 6 years post-natal), the rate of bi-nucleate RPE cells in humans was highest at the equator (4.7 %, ranging from 1.7% to 11.4%), and stable throughout development (Robb, 1985). Thus the frequency and topography of multinucleated RPE cells differ significantly

between humans and rodents, highlighting the limited comparability of posterior poles of mice and humans.

In humans: striking absence of multi-nucleated RPE at the fovea

The nearly complete absence of multi-nucleate cells in the human fovea is striking, underlying the high order of cells in the RPE monolayer at this region. The fovea has the highest density of mono-nuclear, hexagonal RPE cells (Ach *et al.*, 2014), which may reflect the specialized needs of foveal cones in sustaining high-acuity vision. The perfect spatial order of RPE cells and photoreceptors might be the prerequisite for optimal photon capture at the fovea center (Williams, 1985). The spacing and geometry of cone packing is optimally balanced for resolution without aliasing except under specific circumstances (Hirsch & Curcio, 1989; Provis *et al.*, 2013). The RPE under the fovea reflects the requirements of cone sampling array by maintaining hexagonality (Ach *et al.*, 2014) and minimal number of nuclei. In contrast, the highest rate of bi-nucleate cells is at the perifovea, in concordance with the highest density of rod photoreceptors. The high density of bi-nucleate cells in the perifovea could either reflect special requirements of the rod photoreceptor metabolism, markers of past developmental processes (closure of optic fissure) (Fleming *et al.*, 1997; Duncker *et al.*, 2012), or other currently unknown mechanisms. Our data is consistent with recent studies of human RPE bisretinoid content (Ablonczy *et al.*, 2013) demonstrating a distinct spatial organization of this epithelium, which should be incorporated in models of cellular health and disease.

Significance of multi-nucleation: still under discussion

In mammals, the majority of cells are diploid with one cell nucleus. Only a few tissues in the human body contain polyploid multi-nucleate cells, i.e., multiple chromosome sets. These include heart (cardiomyocytes) (Walsh *et al.*, 2010), liver (hepatocytes) (Celton-Morizur *et al.*, 2009), and bones (osteoblasts), with the definite significance of these cells still unknown. There are at least two possible mechanisms for polyploidy: cell fusion, which leads to a bi-nucleate cell with two diploid genomes, and cell cycle mechanisms, including atypical DNA replication, dissolving sister-chromatid cohesion, mitotic spindle function, and cytokinesis (Storchova & Pellman, 2004). It remains unclear whether cellular multi-nucleation and polyploidy presented in one cell is a physiological or pathological process.

Multi-nucleation results in a reduced surface-to-cytoplasmic volume ratio for the whole cell, thereby minimizing membrane requirements (Comai, 2005) and maintaining critical nucleus:cytoplasm ratio (Bodenstein & Sidman, 1987). Furthermore, it has been proposed that polyploidization might increase the metabolic capacity of a tissue by “focusing on gene duplication and protein synthesis instead of cell division and membrane synthesis” (Joubès & Chevalier, 2000; Lacroix & Maddox, 2012). Polyploidization increases the transcriptional and translational output of the same set of gene products which are required for a cell type-specific function (Pandit *et al.*, 2013). In this context it is unclear whether polyploidization is causation or association, but it can also lead cell physiology toward specific and more effective functions, as seen in macrophages (Vignery, 2000; Vignery, 2005), myoblast (Abmayr & Pavlath, 2012), and osteoclasts (Teitelbaum & Ross, 2003).

Polyploidization might be a consequence of normal aging and cellular stress, like in hepatocytes in the human liver after age 50 (Kudryavtsev *et al.*, 1993). The comparison of bi-nucleate RPE in two age groups in the current study did not reveal any significant differences; however, earlier changes in the immediate postnatal phase or within the first decades of life cannot be excluded. Feeney reported a significant increase of deposition of autofluorescence lipofuscin granules in the second decade, which might lead to increased metabolic stress and, as a reaction, to polyploidization. Metabolic rate and stress might be especially high at the perifoveal region (highest increase of lipofuscin/melanolipofuscin with age) (Ach *et al.*, 2014).

The distribution of incident light, often invoked as a mechanism behind topographic differences in the retina, is fairly even across the fundus out to 50° of eccentricity and thus does not explain variation within the 6 mm diameter macula (21° of vision) (Kooijman, 1983; Pflibsen *et al.*, 1988; Bone *et al.*, 2012).

In general, RPE cells are believed to be post-mitotic non-dividing cells (Ts'o & Friedman, 1968; Robb, 1985). However, Rappaport et al. reported the presence of occasional 3H-thymidine-labelled RPE cells in monkeys up to 204 postnatal days, which might indicate that a source of additional cells in the mature retina is mitoses within the RPE itself (Rapaport *et al.*, 1995).

Strengths and weaknesses of this study

A strength of our study is the unbiased sampling method, previously used for imaging autofluorescence and cell density in RPE flatmounts. Z-stack imaging allowed us to reliably determine the non-autofluorescent cell nuclei within the vast majority of RPE cells. Future studies will use nucleic acid markers (e.g., 4′,6-Diamidin-2-phenylindol) to increase sample size and enhance detection of multinucleate RPE cells, Ki67 immunohistochemistry and BrdU labeling to confirm cell cycle activity, and transmission electron microscopy to check chromatin structure in polyploid cells. As RPE imaging with cellular resolution continues to develop (Scoles *et al.*, 2014) it is possible that more longitudinal data on multinucleate cells will become available.

Conclusion

In conclusion, we have demonstrated for the first time that multi-nucleate RPE cells show a characteristic distribution pattern within the macula. Their near-absence in the fovea may reflect the specialized needs of foveal cones in sustaining high-acuity vision, while the high frequency of multi-nucleate RPE cells at the perifovea might reflect specific requirements of retinal metabolism, markers of past developmental processes, and other mechanisms to be explored in further studies.

Supplementary Material

Refer to Web version on PubMed Central for supplementary material.

Acknowledgments

The authors thank Kristen M Hammack for her assistance with the custom FIJI plugin. This study was supported by grants from the German Research Foundation DFG (Bonn, Germany) #AC265/1-1 and #AC265/2-1 (both TA), National Institutes of Health (Bethesda, Maryland, USA) Grants R01 EY06109 (CAC), R01 EY015520 (RTS), EY019065 (ZA), Research to Prevent Blindness (CAC, ZA; New York, New York, USA), EyeSight Foundation of Alabama (CAC; Birmingham, Alabama, USA).

Literature

Ablonczy Z, Higbee D, Anderson DM, Dahrouj M, Grey AC, Gutierrez D, Koutalos Y, Schey KL, Hanneken A, Crouch RK. Lack of Correlation Between the Spatial Distribution of A2E and Lipofuscin Fluorescence in the Human Retinal Pigment Epithelium. Investigative ophthalmology & visual science. 2013; 54:5535–5542. [PubMed: 23847313]

Abmayr SM, Pavlath GK. Myoblast fusion: lessons from flies and mice. Development. 2012; 139:641–656. [PubMed: 22274696]

Ach T, Huisingh C, McGwin G Jr, Messinger JD, Zhang T, Bentley MJ, Gutierrez DB, Ablonczy Z, Smith RT, Sloan KR, Curcio CA. Quantitative autofluorescence and cell density maps of the human retinal pigment epithelium. Investigative ophthalmology & visual science. 2014; 55:4832–4841. [PubMed: 25034602]

Al-Hussaini H, Kam JH, Vugler A, Semo M, Jeffery G. Mature retinal pigment epithelium cells are retained in the cell cycle and proliferate in vivo. Molecular vision. 2008; 14:1784–1791. [PubMed: 18843376]

Al-Hussaini H, Schneiders M, Lundh P, Jeffery G. Drusen are associated with local and distant disruptions to human retinal pigment epithelium cells. Experimental eye research. 2009; 88:610–612. [PubMed: 18992244]

Bodenstein L, Sidman RL. Growth and development of the mouse retinal pigment epithelium. I. Cell and tissue morphometrics and topography of mitotic activity. Developmental biology. 1987; 121:192–204. [PubMed: 3569658]

Bone RA, Gibert JC, Mukherjee A. Light distributions on the retina: relevance to macular pigment photoprotection. Acta biochimica Polonica. 2012; 59:91–96. [PubMed: 22428119]

Celton-Morizur S, Merlen G, Couton D, Margall-Ducos G, Desdouets C. The insulin/Akt pathway controls a specific cell division program that leads to generation of binucleated tetraploid liver cells in rodents. The Journal of clinical investigation. 2009; 119:1880–1887. [PubMed: 19603546]

Comai L. The advantages and disadvantages of being polyploid. Nature Reviews Genetics. 2005; 6:836–846.

Curcio CA, Sloan KR, Kalina RE, Hendrickson AE. Human photoreceptor topography. The Journal of comparative neurology. 1990; 292:497–523. [PubMed: 2324310]

Ding JD, Johnson LV, Herrmann R, Farsiu S, Smith SG, Groelle M, Mace BE, Sullivan P, Jamison JA, Kelly U, Harrabi O, Bollini SS, Dilley J, Kobayashi D, Kuang B, Li W, Pons J, Lin JC, Bowes Rickman C. Anti-amyloid therapy protects against retinal pigmented epithelium damage and vision loss in a model of age-related macular degeneration. Proceedings of the National Academy of Sciences of the United States of America. 2011; 108:E279–287. [PubMed: 21690377]

Duncker T, Greenberg JP, Sparrow JR, Smith RT, Quigley HA, Delori FC. Visualization of the optic fissure in short-wavelength autofluorescence images of the fundus. Investigative ophthalmology & visual science. 2012; 53:6682–6686. [PubMed: 22956617]

Feeney L. Lipofuscin and melanin of human retinal pigment epithelium. Fluorescence, enzyme cytochemical, and ultrastructural studies. Investigative ophthalmology & visual science. 1978; 17:583–600. [PubMed: 669890]

Fleming PA, Harman AM, Beazley LD. Changing topography of the RPE resulting from experimentally induced rapid eye growth. Visual neuroscience. 1997; 14:449–461. [PubMed: 9194313]

Hirsch J, Curcio CA. The spatial resolution capacity of human foveal retina. Vision research. 1989; 29:1095–1101. [PubMed: 2617858]

Joubès, J.; Chevalier, C. The Plant Cell Cycle. Springer; 2000. Endoreduplication in higher plants; p. 191-201.

Kooijman AC. Light distribution on the retina of a wide-angle theoretical eye. J Opt Soc Am. 1983; 73:1544–1550. [PubMed: 6644400]

Kudryavtsev B, Kudryavtseva M, Sakuta G, Stein G. Human hepatocyte polyploidization kinetics in the course of life cycle. Virchows Archiv B. 1993; 64:387–393.

Lacroix B, Maddox AS. Cytokinesis, ploidy and aneuploidy. The Journal of pathology. 2012; 226:338–351. [PubMed: 21984283]

Pandit SK, Westendorp B, de Bruin A. Physiological significance of polyploidization in mammalian cells. Trends in cell biology. 2013; 23:556–566. [PubMed: 23849927]

Pflibsen KP, Pomerantzeff O, Ross RN. Retinal illuminance using a wide-angle model of the eye. J Opt Soc Am A. 1988; 5:146–150. [PubMed: 3351651]

Provis JM, Dubis AM, Maddess T, Carroll J. Adaptation of the central retina for high acuity vision: cones, the fovea and the avascular zone. Progress in retinal and eye research. 2013; 35:63–81. [PubMed: 23500068]

Rapaport DH, Rakic P, Yasamura D, LaVail MM. Genesis of the retinal pigment epithelium in the macaque monkey. The Journal of comparative neurology. 1995; 363:359–376. [PubMed: 8847405]

Robb RM. Regional changes in retinal pigment epithelial cell density during ocular development. Investigative ophthalmology & visual science. 1985:614–620. [PubMed: 3997415]

Scoles D, Sulai YN, Langlo CS, Fishman GA, Curcio CA, Carroll J, Dubra A. In vivo imaging of human cone photoreceptor inner segments. Investigative ophthalmology & visual science. 2014; 55:4244–4251. [PubMed: 24906859]

Shi G, Maminishkis A, Banzon T, Jalickee S, Li R, Hammer J, Miller SS. Control of chemokine gradients by the retinal pigment epithelium. Investigative ophthalmology & visual science. 2008; 49:4620–4630. [PubMed: 18450597]

Storchova Z, Pellman D. From polyploidy to aneuploidy, genome instability and cancer. Nature reviews Molecular cell biology. 2004; 5:45–54. [PubMed: 14708009]

Strauss O. The retinal pigment epithelium in visual function. Physiological reviews. 2005; 85:845–881. [PubMed: 15987797]

Teitelbaum SL, Ross FP. Genetic regulation of osteoclast development and function. Nature Reviews Genetics. 2003; 4:638–649.

Ts'o MO, Friedman E. The retinal pigment epithelium. I. Comparative histology. Archives of ophthalmology. 1967; 78:641–649. [PubMed: 4963693]

Ts'o MO, Friedman E. The retinal pigment epithelium. 3. Growth and development. Archives of ophthalmology. 1968; 80:214–216. [PubMed: 5661888]

Vignery A. Osteoclasts and giant cells: macrophage-macrophage fusion mechanism. International journal of experimental pathology. 2000; 81:291–304. [PubMed: 11168677]

Vignery A. Macrophage fusion the making of osteoclasts and giant cells. The Journal of experimental medicine. 2005; 202:337–340. [PubMed: 16061722]

Walsh S, Ponten A, Fleischmann BK, Jovinge S. Cardiomyocyte cell cycle control and growth estimation in vivo--an analysis based on cardiomyocyte nuclei. Cardiovascular research. 2010; 86:365–373. [PubMed: 20071355]

Wang L, Li CM, Rudolf M, Belyaeva OV, Chung BH, Messinger JD, Kedishvili NY, Curcio CA. Lipoprotein particles of intraocular origin in human Bruch membrane: an unusual lipid profile. Investigative ophthalmology & visual science. 2009; 50:870–877. [PubMed: 18806290]

Williams DR. Aliasing in human foveal vision. Vision research. 1985; 25:195–205. [PubMed: 4013088]

Ziegler A, Kastner C, Blettner M. The Generalised Estimating Equations: An Annotated Bibliography. Biometrical Journal. 1998; 40:115–139.

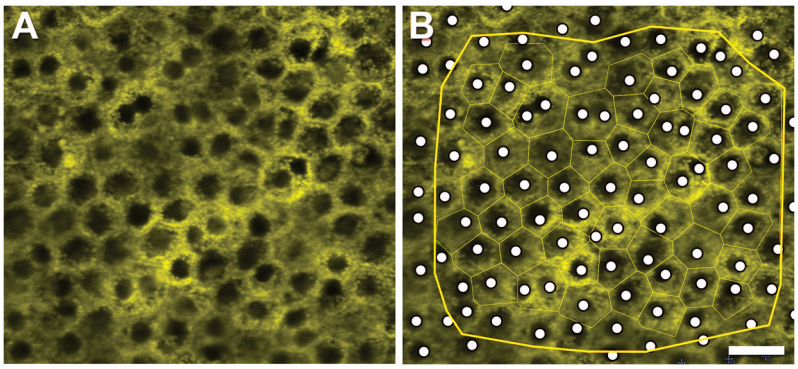

Figure 1. Computer-assisted manual marking of cell nuclei

A Single image from z-stack before marking. **B** Single image from z-stack with Voronoi regions (surrogate for cells, *thin green borders* around cells) displayed and cell nuclei identified (*white dots*). All data within *yellow edging* were used for analysis. As previously described, (Ach *et al.*, 2014) Voronoi regions (collection of regions that tessellate a plane) were generated from corresponding RPE cytoskeleton images (not shown). Scale bar: 20 μm.

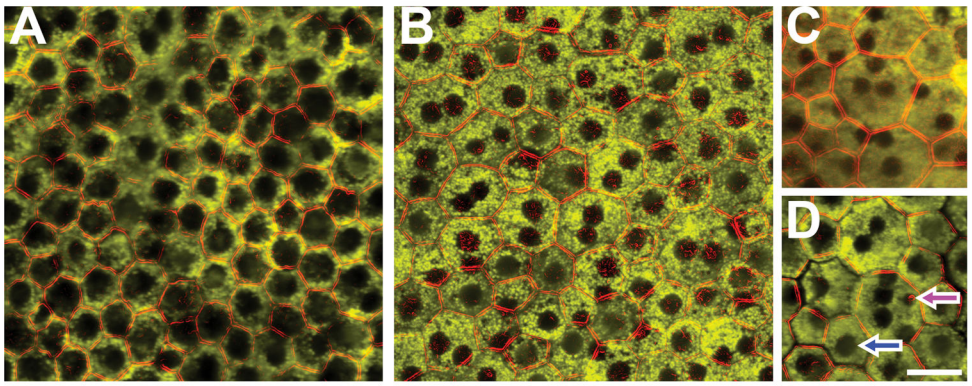

Figure 2. RPE cells with one (A) or multiple (B–D) cell nuclei in normal human macula

There are mono- (A) and fewer bi-nucleate (B) RPE cells visible throughout the macula. Only a few cells with ≥3 nuclei were detectable: tri-nucleate (C) and penta-nucleate (D). Cells in regions with a high percentage of bi-nucleate RPE cells are pleomorphic in size and shape. Of note in (D), cell nuclei differ in size (blue arrow: nucleus size comparable to nuclei in surrounding cells; magenta arrow: a noticeably smaller nucleus). Foveal cells in panel A have abundant, apically located melanosomes which can be mistaken for large nuclei. **A** Temporal perifovea, female, 41 years. **B** Nasal near periphery, female, 37 years. **C** Superior near periphery, male, 88 years. **D** Superior perifovea, female, 50 years. Scale bar 20 μm

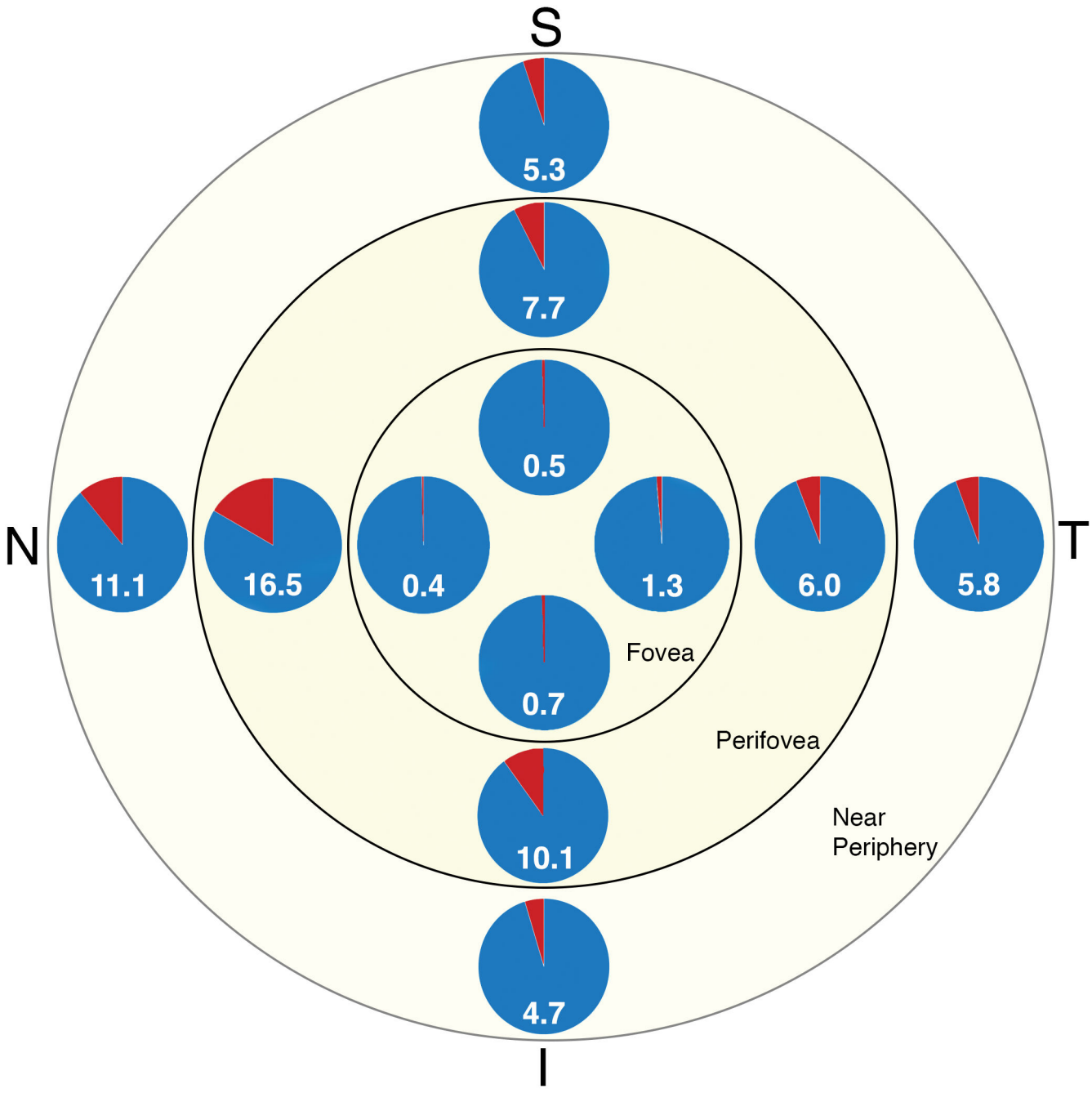

Figure 3. Percentages of multi-nucleate RPE cells as a function of eccentricity and quadrant

The percentage of multi-nucleate RPE cells at each location, i.e., quadrant at each eccentricity, is presented in this multi pie illustration: as number and area (red) of each pie. Cells were pooled across all tissues. Quadrant (T = temporal, S = superior, N = nasal, I = inferior)

Table 1

Absolute numbers, percentages, and number of nuclei/cell in RPE cells of the human macula.

	Absolute numbers			Percentage		Number of nuclei/cell		
	Cells analyzed	Mono-nucleate	Multi-nucleate	Mono-nucleate	Multi-nucleate	Mean	Std Dev	Range
≤ 51 years	5378	5083	295	94.51	5.49	1.06	0.23	1 – 3
>80 years	6025	5711	314	94.79	5.21	1.05	0.23	1 – 5
Fovea	4618	4584	34	99.26	0.74	1.01	0.09	1 – 2
Perifovea	3893	3508	385	90.11	9.89	1.10	0.30	1 – 3
Near periphery	2892	2702	190	93.43	6.57	1.07	0.26	1 – 5
I	2660	2531	129	95.15	4.85	1.05	0.21	1 – 2
N	2751	2522	229	91.68	8.32	1.08	0.28	1 – 3
S	3193	3056	137	95.71	4.29	1.04	0.20	1 – 3
T	2799	2685	114	95.93	4.07	1.04	0.21	1 – 5
Female	7652	7259	393	94.86	5.14	1.05	0.23	1 – 5
Male	3751	3535	216	94.24	5.76	1.06	0.24	1 – 3

I = inferior; N = nasal; S = superior; T = temporal; Std Dev = standard deviation.

Table 2

Percentages of multi-nucleate cells in each quadrant at each eccentricity and the inter-quadrant (superior, inferior, nasal, temporal) and inter-eccentricity (fovea, perifovea, near periphery) significances.

	Fovea	Perifovea	Periphery	*p-value*[1]	*p-value*[2]	*p-value*[3]
Inferior	**0.71**	**10.12**	**4.71**	*<0.0001*	*0.0185*	*0.0249*
Nasal	**0.42**	**16.45**	**11.08**	*<0.0001*	*<0.0001*	*0.0231*
Superior	**0.50**	**7.66**	**5.26**	*0.0002*	*0.0016*	*0.0813*
Temporal	**1.33**	**6.00**	**5.79**	*0.0004*	*0.0046*	*0.7590*
p-value[4]	*0.4030*	*0.0002*	*0.0312*			
p-value[5]	*0.6049*	*0.0088*	*0.8245*			
p-value[6]	*0.2788*	*0.0001*	*0.6226*			
p-value[7]	*0.6473*	*<0.0001*	*0.0012*			
p-value[8]	*0.2136*	*<0.0001*	*0.0185*			
p-value[9]	*0.2150*	*0.2434*	*0.4352*			

p-value[1] compares fovea vs. perifovea

p-value[2] compares fovea vs. periphery

p-value[3] compares perifovea vs. periphery

p-value[4] compares inferior vs. nasal

p-value[5] compares inferior vs. superior

p-value[6] compares inferior vs. temporal

p-value[7] compares nasal vs. superior

p-value[8] compares nasal vs. temporal

p-value[9] compares superior vs. temporal